J|A|C|S ARTICLES

Published on Web 07/13/2010

Biphasic Pd−Au Alloy Catalyst for Low-Temperature CO Oxidation

Jing Xu,[†] Tim White,[‡] Ping Li,[†] Chongheng He,[†] Jianguo Yu,[†] Weikang Yuan,[†] and Yi-Fan Han*,[†]

State Key Laboratory of Chemical Engineering, East China University of Science and Technology, Shanghai 200237, People's Republic of China, and Centre for Advanced Microcopy, Australian National University, Canberra, ACT 2601, Australia

Received March 30, 2010; E-mail: yifanhan@ecust.edu.cn

Abstract: Low-temperature CO oxidation over a compositional series of Pd−Au nanoalloy catalysts supported on silica fume was studied. Except for the pure metals, these materials invariably showed biphasic separation into palladium- and gold-rich components. Performance was optimal for a catalyst of bulk composition Pd_4Au_1, a mixture of $Pd_{90}Au_{10}$ (72.5 at. %) and $Pd_{31}Au_{69}$ (27.5 at. %), that was remarkably active at 300 K and more stable than a pure Au catalyst. For bulk materials dominated by Pd (Pd:Au = 16:1; 8:1; 4:1), the palladium-rich alloy fraction frequently adopted hollow sphere or annular morphology, while the gold-rich crystals were often multiply twinned. Quantitative powder X-ray diffraction (XRD) showed that under the synthesis conditions used, the Au solubility limit in Pd crystals was ~12 at. %, while Pd was more soluble in Au (~31 at. %). This was consistent with X-ray photoelectron spectroscopy (XPS), which revealed that the surfaces of Pd-rich alloys were enriched in gold relative to the bulk composition. In situ Fourier transform infrared spectra collected during CO oxidation contained a new band at 2114 cm^{-1} (attributed to linear CO−Au/Au−Pd bonds) and reduced intensity of a band at 2090 cm^{-1} (arising from a linear CO−Pd bond) with escalating Au content, indicating that the Pd sites became increasingly obscured by Au. High-resolution electron micrographs (HRTEM) of the Pd-rich alloys revealed atomic scale surface defects consistent with this interpretation. These results demonstrate that gold-containing biphasic Pd nanoalloys may be highly durable alternatives for a range of catalytic reactions.

1. Introduction

The burgeoning demand for clean and energy-efficient chemical processes requires the catalysts of tomorrow to deliver greater activity and selectivity at lower temperatures. Alloys have proven superior to single metal catalysts in this respect for many applications,[1−7] and the pronounced synergistic enhancement of supported bimetallic palladium−gold catalysts is exploited industrially for vinyl acetate (VA) synthesis.[2] These alloys are also superior to pure palladium for CO oxidation,[3,8] coupling acetylene to benzene,[9] hydrogen peroxide synthesis,[10−12] and solvent-free oxidation of primary alcohols to aldehydes.[13] The promotional effects of gold on/in palladium have been extensively examined by several groups;[5,14−19] the Goodman group postulates that Au atoms tune Pd−Pd bonds in model bimetallic compounds via an "ensemble effect" that enhances catalytic performance.[2,17−19] However, due to so-called "material and pressure gaps" between the ideal and real catalytic

[†] East China University of Science and Technology.
[‡] Australian National University.

(1) Alexeev, O. S.; Gates, B. C. *Ind. Eng. Chem. Res.* **2003**, *42*, 1571.
(2) Han, Y.-F.; Wang, J.-H.; Kumar, D.; Goodman, D. W. *J. Catal.* **2005**, *232*, 467.
(3) Scott, R. W.; Sivadinarayana, C.; Wilson, O. M.; Yan, Z.; Goodman, D. W.; Crooks, R. M. *J. Am. Chem. Soc.* **2005**, *127*, 1380.
(4) Besenbacher, F.; Chorkendorff, I.; Clausen, B. S.; Hammer, B.; Molenbroek, A. M.; Nørskov, J. K.; Stensgaard, I. *Science* **1998**, *279*, 1913.
(5) Sinfelt, J. H. *Bimetallic Catalysts: Discovery, Concepts and Application*; Wiley: New York, 1983.
(6) Huber, G. W.; Shabaker, J. W.; Dumesic, J. A. *Science* **2003**, *300*, 2075.
(7) Ksar, F.; Ramos, L.; Keita, B.; Nadjo, L.; Beaunier, P.; Remita, H. *Chem. Mater.* **2009**, *21*, 3677.
(8) Venezia, A. M.; Liotta, L. F.; Pantaleo, G.; La Parola, V.; Deganello, G.; Beck, A.; Koppany, Zs.; Frey, K.; Horvath, D.; Guczi, L. *Appl. Catal., A* **2003**, *251*, 359.
(9) Baddeley, C. J.; Tikhov, M.; Hardacre, C.; Lomas, J. R.; Lambert, R. M. *J. Phys. Chem.* **1996**, *100*, 2189.
(10) Schaak, R. E.; Sra, A. K.; Leonard, B. M.; Cable, R. E.; Bauer, J. C.; Han, Y.-F.; Means, J.; Teizer, W.; Vasquez, Y.; Funck, E. S. *J. Am. Chem. Soc.* **2005**, *127*, 3506.
(11) Landon, P.; Collier, P. J.; Papworth, A. J.; Kiely, C. J.; Hutchings, G. J. *Chem. Commun.* **2002**, 2058.
(12) Han, Y.-F.; Zhong, Z.; Ramesh, K.; Chen, F.; Chen, L.; White, T.; Tay, Q.; Nurbaya Yaakub, S.; Wang, Z. *J. Phys. Chem. C* **2007**, *111*, 8410.
(13) Enache, D. I.; Edwards, J. K.; Landon, P.; Solsona-Espriu, B.; Carley, A. F.; Herzing, A. A.; Watanabe, M.; Kiely, C. J.; Knight, D. W.; Hutchings, G. J. *Science* **2006**, *311*, 362.
(14) Soto-Verdugo, V.; Metiu, H. *Surf. Sci.* **2007**, *601*, 5332.
(15) Maroun, F.; Ozanam, F.; Magnussen, O. M.; Behm, R. J. *Science* **2001**, *293*, 1811.
(16) Gao, F.; Wang, Y.; Goodman, D. W. *J. Am. Chem. Soc.* **2009**, *131*, 5734.
(17) Yi, C.-W.; Luo, K.; Wei, T.; Goodman, D. W. *J. Phys. Chem. B* **2005**, *109*, 18535.
(18) Chen, M.-S.; Kumar, D.; Yi, C.-W.; Goodman, D. W. *Science* **2005**, *310*, 291.
(19) Wei, T.; Wang, J.; Goodman, D. W. *J. Phys. Chem. C* **2007**, *111*, 8781.

10.1021/ja102617r

systems, the practical relevance of these conclusions is difficult to assess, and the surface structure of gold-modified palladium remains conjectural. Furthermore, the precise mechanistic role of gold in accelerating low-temperature reactions remains ambiguous.

The recent enforcement of strict automotive emission controls in the United States and European Union has provided the impetus for the development of green vehicles that employ hydrogen fuel cells driven or biofuel blends that moderate CO release. However, for these approaches to be viable, it will be essential to find highly efficient low-temperature CO oxidation catalysts for purifying H_2 supplying to fuel cells, in which CO (>100 ppm) as a poison tremendously deteriorates the performance of electrocatalysts,[20−22] and for reducing CO emission during cool engine starts that contributes about 90% of the total vehicle discharge.[23]

Many approaches have been explored to develop low-temperature combustion catalysts for treating exhaust gas. The oxidation of CO by supported noble metal[20−25] and Au[26−29] catalysts has been studied for decades, with the latter materials significantly active at/or below room temperature. Presently, gold automotive catalysts show poor durability toward CO_2 and H_2O, and the Au nanoparticles readily aggregate. However, Pd catalysts have proven highly active for CO oxidation at elevated temperatures and are already a vital component of the well-known "three-way catalyst".[3−8,23] Can Pd alloyed with Au bring about an unexpected catalytic performance for low-temperature CO oxidation? To date, improving the low-temperature performance of practical Pd catalyst through alloying with Au for CO oxidation has attracted less attention.[3,8]

In this study, a series of nanocrystalline biphasic Pd−Au alloys were synthesized with the investigation focusing on CO oxidation as a function of bulk catalyst composition, with particular emphasis given to understanding the key role of modified surface chemistries in mixed metal catalysts.[17,30] To minimize strong metal−support interactions (SMSI), and clearly distinguish the role of gold, a nonreducible oxide (SiO_2) scaffold was employed. The crystal domain size and degree of Pd−Au alloying were established by full-pattern quantitative powder X-ray diffraction (XRD), while the morphology, architecture, and dispersion of the particles on the support were inspected by high-resolution transmission electron microscopy (HRTEM). Electronic property modifications of the biphasic Pd/Au catalysts were monitored using the binding energy derived from X-ray photoelectron spectroscopy (XPS) and by in situ diffuse reflection infrared Fourier transform spectroscopy (DRIFTS) during CO adsorption.

2. Experimental Section

2.1. Catalyst Preparation and Reactivity Measurements. Amorphous silica (SiO_2, provided by the Aldrich Chemical Co.) supported Pd, Au, and Pd−Au catalysts were prepared by an incipient wetness method.[9] Salt solutions of Pd^{2+} and Pd^{2+}/Au^{3+} at different metal ratios were prepared by dissolving $Pd(NO_3)_2$ (0.3 M) and $AuCl_3$ (0.3 M) (C.P., commercial sources) in deionized water. Equal volumes of these precursors with equal pore volume of SiO_2 were added to a fumed SiO_2 having a surface area of approximately 230 m^2/g with a particle size range 230−400 mesh and pore volume of 1.1 mL/g. The impregnated samples were allowed to stand for 4 h in a covered beaker before drying overnight under vacuum at 393 K. The Pd loading was maintained at 3.3 wt %. Before CO adsorption or reaction, the catalysts were treated at 673 K in O_2 (20 mL/min) for 30 min, followed by reduction at 573 K in H_2 (20 mL/min), and then they were cooled to room temperature under Ar. The Au/SiO_2 catalyst was treated in O_2 (673 K for 30 min) before reaction for producing metallic Au.

CO oxidation was carried out in a microplug-flow reactor with a feed gas mixture of CO (5.0 kPa), O_2 (5.0 kPa), in Ar with a gas hourly space velocity (GHSV) of 6000−32 000 h^{-1}. To obtain differential reaction rates, CO conversion in whole temperature range was kept below 5% by diluting the catalyst with α-Al_2O_3 powder in ratios ranging from 1 to 20. Absolute mass-specific reaction rates and turnover rates were calculated from the average concentrations ($\dot{c}_i$) of each component, at the inlet and outlet of the reactor:

$$r_{CO} = \frac{\dot{c}_{CO,in} \cdot X_{CO} \cdot \dot{V}_{gas}}{m_{Pd}} [\text{mol min}^{-1}\ \text{g}_{cat}^{-1}] \quad (1)$$

where m_{Pd} is the mass of Pd in the reactor bed, $\dot{V}$ is the total molar flow rate, X_{CO} is the conversion of CO based on CO_2 formation, $\dot{c}_{CO}$ is the concentration of CO in gas mixture, equal to p_i/p_0, p_i is the partial pressure of reactants, and p_0 is the total pressure in the system.

The rates in turnover of frequency (r_{CO}(TOF)/s^{-1}) were calculated as:

$$r_{CO}(\text{TOF}) = \frac{r_{CO} \times M_{Pd}}{D} (s^{-1}) \quad (2)$$

where M_{Pd} is the Pd atom weight, and D is the Pd dispersion calculated from the average size of Pd and Pd−Au nanoparticles.

The reactants and products were analyzed online at 2 h intervals using a gas chromatograph (GC) (Shimadzu GC-14B) equipped with a carbosieves-II column. Relevant details have been given elsewhere.[2] To better understand the response of the materials in use, the time-dependent catalysts reaction was studied in both an ideal gas mixture (5.0 kPa CO, 5.0 kPa O_2, and Ar balance) and a simulated exhaust gas (5.0 kPa CO, 5.0 kPa O_2, 10.0 kPa H_2O, 20.0 kPa CO_2, and Ar balance).

2.2. TPSR CO Oxidation, CO-TPD. The temperature-programmed surface-reaction (TPSR) CO oxidation (5.0 kPa CO in Ar) and temperature-programmed desorption (TPD) of CO experiments were performed in a micro fixed-bed reactor connected to a QMS (HPR-20, Hiden Analytical Ltd.). Masses of *m*/*e* 2, 16, 18, 28, 32, and 44 were monitored; the detection limit in Ar is 100 ppm for CO, 10 ppm for CO_2 and H_2, and less than 1 ppm for O_2. The temperature was ramped from room temperature to 873 K linearly (20 K/min) in a carrier gas (Ar) introduced at a rate of 20 mL/min.

2.3. Materials Characterization. 2.3.1. TEM. The catalyst powders were lightly ground, ultrasonically dispersed in ethanol, and several drops of suspension were loaded on holey carbon films supported by copper grids. Bright-field images were collected at 200 keV using a JEOL 2010 microscope fitted with an ultra high-resolution pole piece. High-resolution images were collected using

(20) Han, Y.-F.; Kahlich, M. J.; Kinne, M.; Behm, R. J. *Phys. Chem. Chem. Phys.* **2002**, *4*, 389.
(21) Han, Y.-F.; Kahlich, M. J.; Kinne, M.; Behm, R. J. *Appl. Catal., B* **2004**, *50*, 209.
(22) Han, Y.-F.; Kinne, M.; Behm, R. J. *Appl. Catal., B* **2004**, *52*, 123.
(23) Collins, N. R.; Twigg, M. V. *Top. Catal.* **2007**, *42−43*, 323.
(24) Engel, T.; Ertl, G. *Adv. Catal.* **1979**, *28*, 1.
(25) Chen, M. S.; Cai, Y.; Yan, Z.; Gath, K. K.; Axnanda, S.; Goodman, D. W. *Surf. Sci.* **2007**, *601*, 5326.
(26) Berlowitz, P. J.; Peden, C. H. F.; Goodman, D. W. *J. Phys. Chem.* **1988**, *92*, 5213.
(27) Haruta, M. *Catal. Today* **1996**, *36*, 153.
(28) Okumura, M.; Nakamura, S.; Tsubota, S.; Nakamura, T.; Azuma, M.; Haruta, M. *Catal. Lett.* **1998**, *51*, 53.
(29) Han, Y.-F.; Zhong, Z.; Ramesh, K.; Chen, F.; Chen, L. *J. Phys. Chem. C* **2007**, *111*, 3163.
(30) Chen, C.-H.; Sarma, L. S.; Chen, J.-M.; Shih, S.-C.; Wang, G.-R.; Liu, D.-G.; Tang, M.-T.; Lee, J.-F.; Hwang, B.-J. *Nano* **2007**, *1*, 114.

Table 1. Properties of Biphasic Pd−Au Alloy Catalysts toward Low-Temperature CO Oxidation[a]

bulk composition		alloy components			materials properties			catalytic activity	
Pd:Au	at. % Au	composition	at. % of alloy	cell constant (Å)	XRD crystal size (nm)	TEM particle size (nm)	surface composition Pd:Au	$T_{20\%}$ (K)	E_a (kJ/mol)
1:0	0	Pd	100	3.8919	20	5−20	NA	413	65.6
16:1	5.9	$Pd_{95}Au_5$	93.2	3.8988	12	5−30	8.2/1	397	53.5
		$Pd_{13}Au_{87}$	6.8	4.0511	10				
8:1	11.1	$Pd_{92}Au_8$	86.5	3.9042	10	5−20	6.8/1	366	67.1
		$Pd_{19}Au_{81}$	13.5	4.0399	8				
4:1	20.0	$Pd_{90}Au_{10}$	72.5	3.9093	4	5−10	3.6/1	337	66.5
		$Pd_{31}Au_{69}$	27.5	4.017	5				
2:1	33.3	$Pd_{89}Au_{11}$	61	3.9096	6	5−20	2.4/1	428	72.3
		$Pd_{23}Au_{77}$	39	4.0312	6				
1:1.16	51.3	$Pd_{88}Au_{12}$	32.5	3.9120	4	10−30	1/1.2	448	116.3
		$Pd_{30}Au_{70}$	67.5	4.0192	8				
1:3.4	77.3	$Pd_{97}Au_3$	20	3.8957	5	10	1/1.5	459	100
		$Pd_{12}Au_{88}$	80	4.0519	12				
0:1	100	Au	100	4.0760	8	10	NA	322	41.3

[a] All experiments were carried out in feed gas of 5 kPa CO, 5 kPa O_2, and the balance Ar (GHSV: 32 000 h^{-1}).

an objective aperture of 20 μm, corresponding to a nominal point-to-point resolution of 0.17 nm. Digital filtering and tests for local symmetry were carried out using Fourier filtering methods as implemented in CRISP.[31] The composition of the metal particles was semiquantitatively analyzed by energy dispersive spectroscopy (EDS) using Au L (21.13 keV) and Pd K (2.84 keV) X-rays. Line scans across individual particles were performed in scanning transmission electron microscope (STEM) mode to probe hollow shell and annular structures.

2.3.2. XRD. Powder X-ray diffraction patterns were accumulated with a Bruker D8 diffractometer using Cu Kα radiation using a step-size of 0.02° 2θ over the range 30−120°. Approximately 10 wt % of standard Si (NIST 640a, $a = 5.40825$ Å) was mixed with the catalysts to allow the accurate determination of lattice constants. The whole pattern was analyzed using the Rietveld method as implemented in TOPAS-V2 with palladium[32] and gold[33] employed as crystallographic starting models. To establish the degree of alloying, the following refinement sequence was employed: a $1/x$ background function and a Chebychev polynomial of order 4 was fitted; the lattice constant of the silicon standard was fixed and the zero shift and scale factor optimized; for the Au-rich and Pd-rich alloys, the lattice parameters, scale factors, metal scattering strengths, and crystallite size were optimized in turn. The isothermal vibration parameters of all phases were fixed at 1.0 Å.

2.3.3. XPS. X-ray photoelectron spectra were collected with a VG ESCALAB 250 spectrometer, using Al K_α radiation (1486.6 eV, pass energy 20.0 eV) at a base pressure of 1×10^{-9} Torr. The background contribution (obtained by the Shirley method) arising from inelastic processes was subtracted, while curve-fitting employed a Gaussian−Lorentzian profile. The binding energies (BEs) were calibrated internally against Si 2p (103.5 eV) and C 1s (285.0 eV) peaks, and externally with a Au wire (Au 4f at 84.0 eV). The reduced catalysts were protected by ultra high purity N_2 when cooling to room temperature. Because of the overlap of the core-level energies of Pd and Au, the determination of Pd and Au chemical states in Pd−Au alloys was referenced against the XPS spectra of Pd 3d over clean single crystal Pd(100) and Au 4f over a Au wire. To eliminate systematic errors, the reference materials were cleaned by Ar ion etching for 5 min at 3.0 μA. The atom ratios of Pd/Au in the alloy surface have been calculated from the equation:[36] $(N_{Pd})/(N_{Au}) = (I_{Pd}/S_{Pd})/(I_{Au}/S_{Au})$, where the I_{Pd} and I_{Au} are the time-normalized intensities of the Pd 3d and Au 4f levels, and S_{Pd} (4.642 for Pd 3d) and S_{Au} (5.24 for Au 4f) are the atomic sensitivity factors for X-ray sources at 90°.

2.3.4. DRIFTS. In situ diffuse reflection infrared Fourier transform spectroscopy was used to quantify CO adsorption on the fresh catalysts in the reaction cell (modified Harricks model HV-DR2) that allowed continuous gas flow through the catalyst bed (ca. 0.1 g) during spectral acquisition. Prior to analysis, the catalysts were treated at 673 K in O_2 (20 mL/min) for 30 min followed by reduction at 573 K in H_2 in the same way; for the Au/SiO_2 catalyst, metallic Au was obtained by treating the precursor in O_2 for 30 min at 673 K. Single beam spectra were collected at room temperature (Bio-Rad FT-IR 3000 MX) at a resolution of 4 cm^{-1} to enhance the extremely low intensity of the CO vibration on the bimetallic Pd−Au surfaces. All spectroscopy was recorded at room temperature.

3. Results and Discussion

3.1. Characterization. XRD and TEM. In equilibrated Pd−Au alloys prepared by casting and annealing, the cell constant increases with Au content.[34,35] However, the nanosized catalyst crystals are far from equilibrated and, invariably, contain Pd−Au particles segregated into two phases (Table 1, Figure 1a,b). Maeland and Flanagan[34] found only a slight deviation from Vegard's Law in equilibrated material across the entire compositional series (not exceeding 0.0046 Å at the Au-rich end), and, therefore, the experimentally determined cell edge a is determined to high accuracy and correlates with stoichiometry according to the relationship at. % Au $= 539.96a - 2100.1$, and the chemistry of the alloy pairs may be determined. Moreover, as the bulk catalyst composition is known, the proportions of each alloy can be established (Table 1, Figure 2a,b). Under the synthesis employed, the solubility of Au in Pd never exceeded 12 at. %, while Pd was somewhat more soluble in Au to a maximum of 31 at. %, with mixing most evident at near equal proportions of Au and Pd overall.

In general, the alloy pairs were of similar size regardless of composition and generally larger toward the end numbers or pure metals (Figure 2) for each composition (Table 1). Usually, there was concurrence between crystal size determined by XRD and the particle size as observed by TEM, and these parameters can be considered equivalent. However, the larger Au-rich particles were often multiply twinned, while such features were rare in the Pd-rich alloys (Figure 3). In addition, in the Pd-rich region (16:1, 8:1, 4:1), the Pd-rich alloys appear to develop as

(31) Hovmöller, S. *Ultramicroscopy* **1992**, *41*, 121.
(32) King, H. W.; Manchester, F. D. *J. Phys. F* **1978**, *8*, 15.
(33) Straumanis, M. E. *Monatsh. Chem.* **1971**, *102*, 1377.
(34) Maeland, A.; Flanagan, T. B. *Can. J. Phys.* **1964**, *42*, 2364.
(35) Venudhar, Y. C.; Iyengar, L.; Krishna Rao, K. V. *J. Less-Common Met.* **1978**, *58*, 55.
(36) Moulder, J. F.; Stickle, W. F.; Sobol, P. E.; Bomben, K. D. In *Handbook of X-ray Photoelectron Spectroscopy*; Chastain, J., King, C., Jr., Eds.; Physical Electronics, Inc., 1995; ISBN: 0-9648124-1-X.

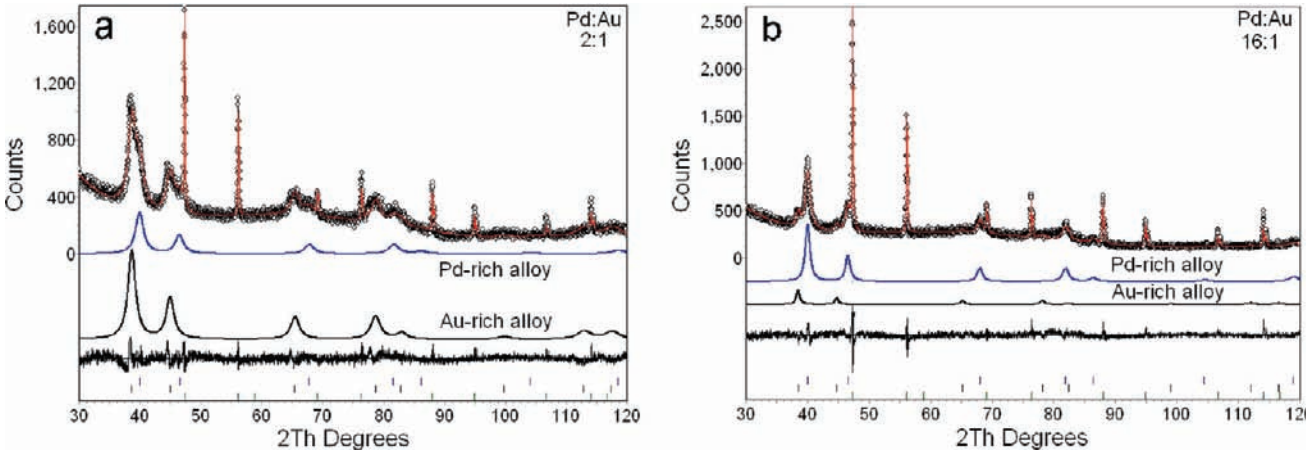

Figure 1. Rietveld analysis showed that for all Pd/Au ratios the X-ray powder diffraction pattern could be separated into two components, a palladium-rich and a gold-rich alloy. (a) For Pd:Au = 2:1, the gold-rich phase is dominant (as gold scatters X-rays more effectively than palladium). The upper portion of the figure is an overlay of experimental and simulated patterns, while the simulated alloy traces are separated below. Lowermost is the difference plot (experimental − calculated) and the Bragg reflection markers. (b) A similar analysis for the catalyst with bulk composition Pd:Au = 16:1. In both cases, the intense narrow reflections arise from the internal silicon standard.

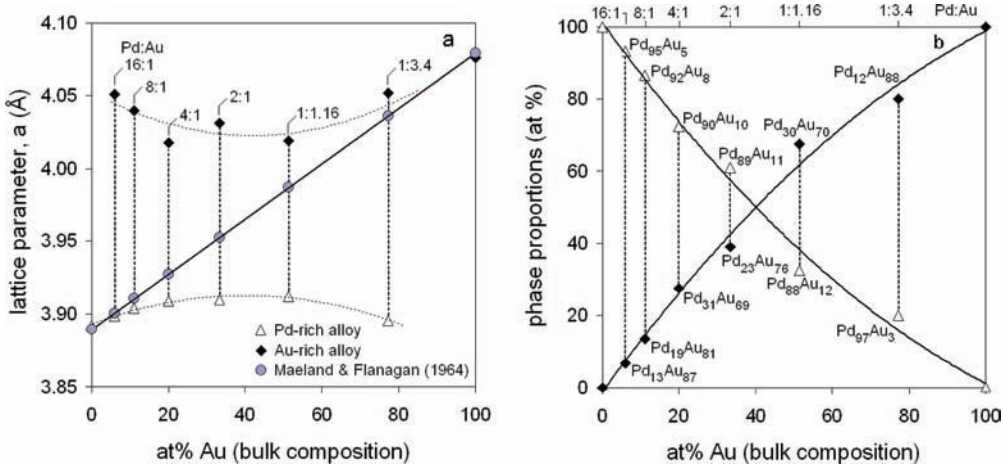

Figure 2. (a) Relationship between alloy lattice parameters and bulk compositions. For comparison, the lattice parameters for single-phase Pd/Au alloys with compositions identical to the bulk composition are included. It is apparent that Pd/Au mixing is maximized when more equal portions of the metals are present; however, clearer (but imperfect) separation into the metals occurs at the composition extremities. (b) The proportions of palladium-rich and gold-rich alloy required to be consistent with the bulk composition.

hollow spheres that collapse to an annular morphology (Figure 4). In detail, these crystals contain contrast features that have been ascribed to vacant surface sites as suggested by Mejia-Rosales et al. (Figure 5).[37] High-resolution micrographs showed that Au and Pd were generally randomly dispersed throughout the crystals, and, more rarely, ordered superlattices were seen (Figure 6). The core−shell morphologies described earlier[38] in which "pure" Pd is coated with Au could not be identified by microscopy for the material in this study, and the XRD study has clearly demonstrated alloying.

XPS. Comparative X-ray photoelectron spectra were collected from clean bulk metals, supported single metal, and supported bimetallic Pd−Au alloy catalysts. In agreement with previous results from metallic Pd,[39−42] binding energies (BE) were calibrated using clean single crystal Pd(100) surfaces with peaks at 335.0 and 340.1 eV assigned to Pd(0) $3d_{5/2}$ and $3d_{3/2}$, respectively, with full-width-at-half-maximum (fwhm) of about 2.2 eV. Also, a peak at 84.0 eV (fwhm = 1.2 eV) from Au wire could be assigned to Au(0) $4f_{7/2}$.

Because the core levels of Pd and Au overlap [Au(0) $4d_{5/2}$ (333.8 eV) with Pd(0) $3d_{5/2}$ (334.0 eV) and Pd(0) 4s (88.2 eV) with Au(0) $4f_{5/2}$ (87.7 eV)], the chemical states were more conveniently specified from the Pd $3d_{3/2}$ and Au $4f_{7/2}$ levels. The Pd $3d_{3/2}$ peak shifted from 340.3 (Pd-only) to 339.9 eV upon alloying with Au ($Pd_1Au_{1.6}$) (Figure 7A), while a shift from 84.0 to 83.7 eV could be seen for the Au $4f_{7/2}$ (Figure

(37) Mejía-Rosales, S. J.; Fernández-Navarro, C.; Pérez-Tijerina, E.; Blom, D. A.; Allard, L. F.; José-Yacamán, M. *J. Phys. Chem. C* **2007**, *111*, 1256.
(38) Ferrer, D.; Torres-Castro, A.; Gao, X.; Sepúlveda-Guzmán, S.; Ortiz-Méndez, U.; José-Yacamán, M. *Nano Lett.* **2007**, *7*, 1701.
(39) Leisenberger, F. P.; Koller, G.; Sock, M.; Surnev, S.; Rcomsey, M. G.; Netzer, F. P.; Klötzer, B.; Hayek, K. *Surf. Sci.* **2000**, *445*, 380.
(40) Voogt, E. H.; Mens, A. J. M.; Gijzeman, O. L. J.; Geus, J. W. *Surf. Sci.* **1997**, *373*, 210.
(41) Beutler, A.; Sandell, A.; Jaworowski, A. J.; Wiklund, M.; Nyholm, R.; Anderson, J. N. *Surf. Sci.* **1998**, *418*, 457.
(42) Watson, R. E.; Hudis, J.; Periman, M. L. *Phys. Rev. B* **1971**, *4*, 4139.

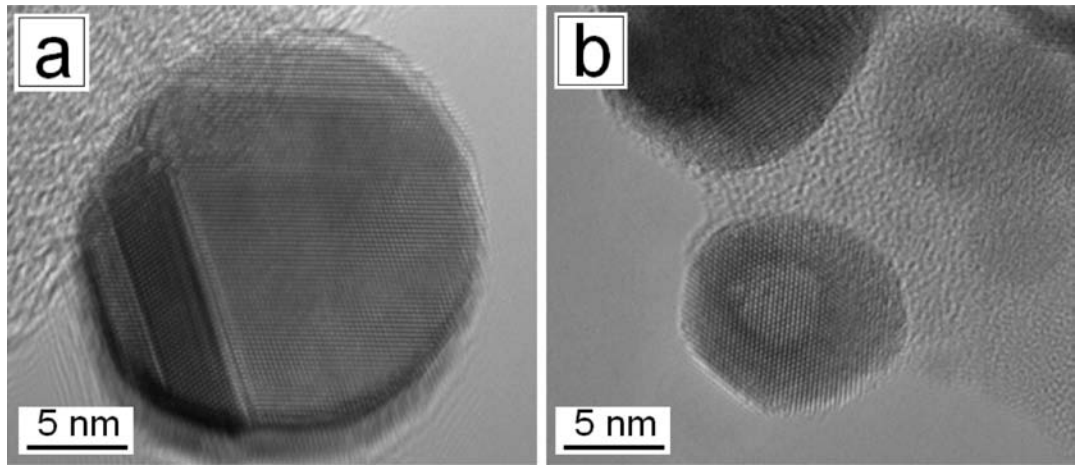

Figure 3. (a) Multiply twinned gold crystal from a catalyst of bulk composition Pd:Au = 1:3.4. (b) Hollow sphere Pd-rich crystal from material of bulk composition Pd:Au = 16:1.

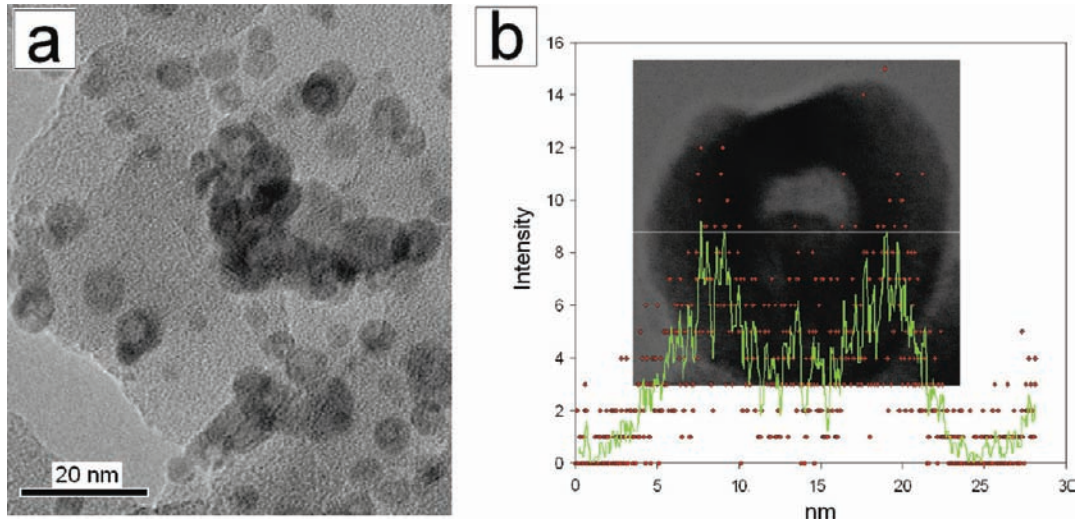

Figure 4. (a) Bright-field TEM image of palladium-rich alloy particles from the catalyst of bulk composition Pd:Au = 16:1 illustrating the common annular structure. Similar morphology was see in Pd:Au = 8:1 and 4:1 materials. (b) An energy dispersive line scan across an annular particle using the Pd-L X-rays. The underlying STEM image provides correspondence between structure and chemistry. The gold signal was too low for a similar line scan in accord with the average alloy composition ($Pd_{95}Au_5$) as determined by X-ray diffraction (Table 1).

7B) over $Pd_1Au_{1.6}$. An upshift of Au 4f was not observed for $Pd_1Au_{3.4}$, probably because a portion of the Au was unalloyed. The lower BEs for both Pd $3d_{3/2}$ and Au $4f_{7/2}$ are consistent with the net charge flowing into Au (higher Au s or p electron densities) and Pd (gaining d electrons from Au),[43−46] indicating the electronic structure of the surface Pd atoms to be modified via alloying with Au, and vice versa.

Generally, Pd in a Pd−Au alloy is more electronegative than Au, even though Au has the greater electronegativity according to Pauling.[47] In Pd−Au alloy, the gain of the Pd valence "d" density is supposed to be compensated by the depletion of core s or p electron count.[44,45] It has been demonstrated that net charge flowing into Au results in a reduction in BE by approximately −0.4 eV for the Au 4f BE when the bulk Au concentration in a Pd−Au alloy is less than 0.5; meanwhile, a shift of ca. −0.1 eV for the Pd 3d BE is due to the gain of d electrons from Au.[44,45]

XPS analysis further revealed that the surfaces in all samples were enriched in Au, as compared to the bulk composition when Pd/Au > 2, and gradually decreased with Au content. Conversely, Pd signal was enhanced from 2:1 < Pd:Au < 1:3.4. Au enrichment in Pd−Au alloy surfaces has also been discussed by Yi et al. in a recent study of model bimetallic Pd−Au catalysts.[17] From XRD, it is evident that there is limited solubility between Au and Pd in the alloy nanocrystals, especially Au in Pd-rich crystals as they are not thermodynamically equilibrated. Therefore, it is perhaps not surprising that surface analysis reflects the relative difficulty of Au dissolving in Pd, and the consequent enrichment.

DRIFTS. The electronic influence of Au on Pd was also examined by in situ DRIFTS during CO adsorption. As shown in Figure 8, the bands at 2090 and 1982 cm^{-1} were observed over pure Pd and Pd−Au alloys up to the bulk atomic ratio

(43) José-Yacamán, M.; Mejía-Rosales, S.; Pérez-Tijerina, E.; Blom, D. A.; Allard, L. F. *Microsc. Microanal.* **2006**, *12*, 772.
(44) Chou, T. S.; Perlman, M. L.; Watson, R. E. *Phys. Rev. B* **1976**, *14*, 3248.
(45) Nascente, P. A. P.; de Castro, S. G. C.; Landers, R.; Kleiman, G. G. *Phys. Rev. B* **1991**, *43*, 4659.
(46) Deki, S.; Akamatsu, K.; Hatakenaka, Y.; Mizuhata, M.; Kajinami, A. *Nano Struct. Mater.* **1999**, *11*, 59.
(47) Pauling, L. *The Nature of the Chemical Bond*, 3rd ed.; Cornell University Press: Ithaca, NY, 1960; p 93.

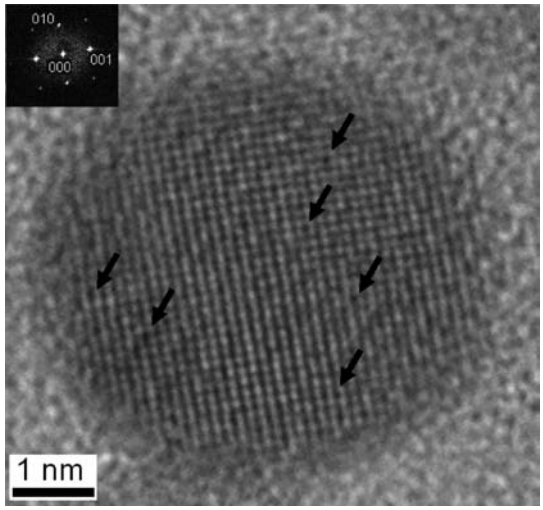

Figure 5. A [100] high-resolution image of a palladium-rich alloy particle in the catalyst of bulk composition Pd:Au = 2:1. In accord with José-Yacamán et al.,[37] atomic-scale features with dark contrast are ascribed to surface site vacancies, some of which are indicated by arrows, and are frequently observed.

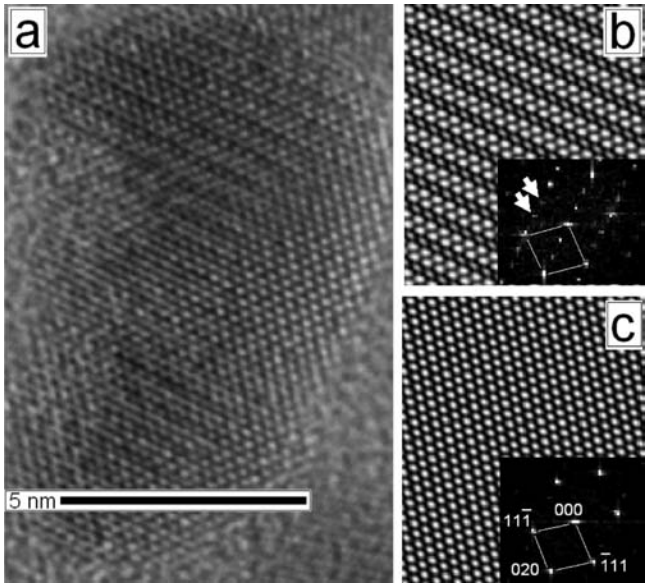

Figure 6. (a) A [101] high-resolution micrograph of a particle in a catalyst of bulk composition Pd:Au = 4:1. While the cubic subcell is clear in the central region of the crystal, a 3x superstructure that propagates along $[020]_s$ is clearly observed in thicker portions. (b) Fourier reconstruction and filtering of the upper part of the micrograph with point symmetry constrained to *p*2 further emphasize the superstructure. The superlattice reflections in the Fourier transform are arrowed. (c) Similar image processing for the central region, where superlattice reflections are absent in reciprocal space; representation shows the subcell only.

Pd_2Au_1, corresponding to linear and bridged adsorbed CO on metallic Pd atoms, respectively.[17,26] The linear CO band shifted to 2080 cm^{-1} for $Pd_1Au_{3.4}$, due to an increase of d orbital electron density in surface Pd, consistent with the BE trends. Simultaneously, a new band appeared at 2114 cm^{-1}, which is assigned to linear adsorbed CO on metallic Au atoms as reported by Schubert et al.[48] To our knowledge, this is the first observation of an infrared CO vibration band on Au-rich bimetallic Pd−Au alloy catalysts. It is noted that the same vibration band has only been reported for the Pd−Au/Mo(110) model catalyst at ∼100 K in a vacuum system.[19]

3.2. Kinetics and TPSR of CO Oxidation. Temperature-dependent CO oxidation was conducted on all catalysts (Figure 9) with the pure Au material showing the greatest activity, even at room temperature (5% conversion of CO at 300 K). Under the same conditions, and on the basis of 20% conversion of CO ($T_{20\%}$, column 4 in Table 1), the activity for Pd−Au alloy catalysts increased from Pd to Pd_4Au_1, and then fell rapidly with increasing Au content to $Pd_1Au_{3.4}$. The activities from highest to lowest for all catalyst pairs were in sequence: Au > Pd:Au = 4:1 > 8:1 > 16:1 > Pd > 2:1 > 1:1.6 > 1:3.4. Arrhenius plots were used to derive the apparent activation energies (E_a) (Figure 10, Table 1), which was 65.6 kJ/mol for pure Pd, and remained constant from Pd to Pd_4Au_1, before increasing rapidly to $Pd_1Au_{3.4}$ (100.0 kJ/mol), then falling to 41.3 kJ/mol for the Au-only catalyst. It is noted that Pd_4Au_1 exhibited superior activity and stability as compared to pure gold, with the latter showing a 50% loss of activity after 10 h at 353 K as compared to 5% for Pd_4Au_1 in an ideal exhaust gas of 5.0 kPa CO, 5.0 kPa O_2, and Ar balance (Figure 11). In addition, in the simulated exhaust gas (5.0 kPa CO, 5.0 kPa O_2, 10.0 kPa H_2O, 20.0 kPa CO_2, and Ar balance), there was a substantial loss of activity for pure Au, while only a mild deterioration was observed for Pd_4Au_1. The Pd_4Au_1 catalyst could oxidize CO at room temperature in a mixture of CO (5.0 kPa) + O_2 (5.0 kPa) + Ar, in a steady-state reaction rate (5.0×10^{-4} s^{-1}) for 10 h.

A TPSR experiment was carried out on the Pd_4Au_1 catalyst to better evaluate Au promotional effects. In this experiment, the evolution of CO_2 was observed during exposure of an O-precovered Pd−Au surface to a stream of CO (5.0 kPa) + Ar (curve A, Figure 12). A CO_2 peak was evident at 300 K within 15 min, with a similar feature appearing for a CO-precovered surface in a stream of O_2 (5.0 kPa) + Ar (curve B, Figure 12). As expected, CO_2 production was more rapid in an oxygen-rich atmosphere (curve B).[2,17] In a subsequent TPSR run (following the experiment in Figure 12), three CO_2 peaks were observed at ca. 383, 483, and 573 K (curve B in Figure 13). The first two peaks may originate from surface reactions between CO_{ad} and O_{ad}, while a third could indicate the dissociative desorption of CO_{ad} (Boudouard reaction), because only a single CO_2 peak at 653 K appeared in the CO-TPD spectrum (curve A in Figure 13). There was no CO_2 formation over the Pd-only and the Au-only catalysts through the same procedure at 300 K.

3.3. Mechanism for CO Oxidation on Pd−Au Alloy Catalysts. Studies concerning low-temperature CO oxidation on supported Pd−Au alloy catalysts are relatively few,[2,3,8,28] and even rarer for pure Pd.[23,49,50] However, supported nanosize Au particles (2−5 nm) are well-known for promoting for CO oxidation at or below room temperature.[27−29] Here, we focus on Au promotional effects. The kinetic study demonstrates that Au considerably enhances Pd catalytic activity, and over the composition range Pd to Pd:Au = 4:1 (a mixture of 72.5% $Pd_{90}Au_{10}$ and 27.5% $Pd_{31}Au_{69}$), the activity of the catalysts improved significantly. Two mechanisms may be responsible:

(i)CO oxidation proceeds at the interface of contiguous ensembles or atoms of pure Pd and pure Au, where Pd and Au have complementary roles. Chen et al.[18] recently pointed out

(48) Schubert, M. M.; Venugopal, A.; Kahlich, M. J.; Plzak, V.; Behm, R. J. *J. Catal.* **2004**, *222*, 32.

(49) Steiner, P.; Hufner, S. *Solid State Commun.* **1982**, *41*, 619.

(50) Han, Y.-F.; Kumar, D.; Sivadinarayana, C.; Clearfield, D.; Goodman, D. W. *Catal. Lett.* **2004**, *94*, 131.

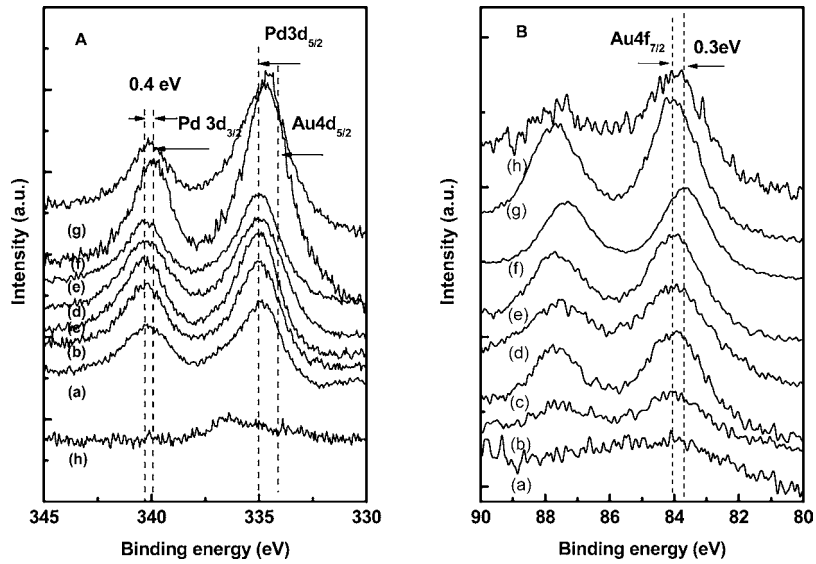

Figure 7. (A) XPS Pd_{3d} spectroscopy and (B) XPS Au_{4f} spectroscopy over the SiO_2 supported Pd−Au alloy catalysts. The change of the atomic ratio of Pd and Au by fixing Pd 3.3 wt % in all catalysts: (a) pure Pd, (b) $Pd_{16}Au_1$, (c) Pd_8Au_1, (d) Pd_4Au_1, (e) Pd_2Au_1, (f) $Pd_1Au_{1.6}$, (g) $Pd_1Au_{3.4}$, and (h) pure Au.

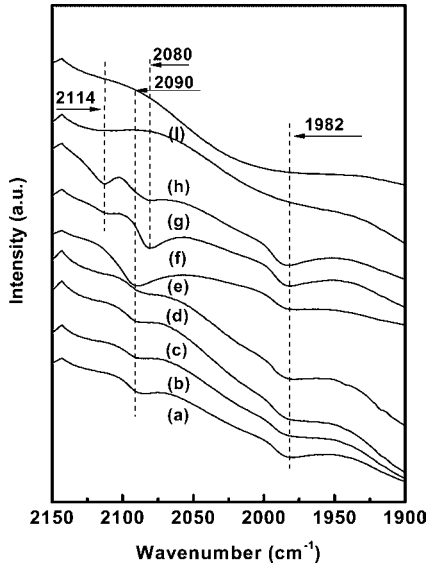

Figure 8. In situ DRIFTS of CO (2.0% in He) adsorption on the SiO_2 supported Pd−Au alloy catalysts at room temperature. The change of the atomic ratio of Pd and Au by fixing Pd 3.3 wt % in all catalysts: (a) pure Pd, (b) $Pd_{16}Au_1$, (c) Pd_8Au_1, (d) Pd_4Au_1, (e) Pd_2Au_1, (f) $Pd_1Au_{1.6}$, (g) $Pd_1Au_{3.4}$, (h) pure Au, and (i) SiO_2.

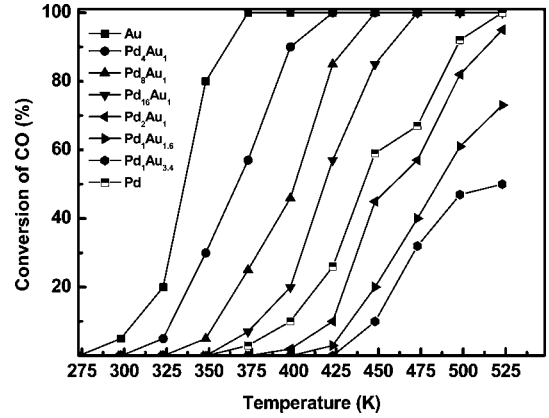

Figure 9. Temperature-dependent CO oxidation over the SiO_2 supported Pd−Au alloy catalysts with a feed gas of 5.0 kPa CO, 5.0 kPa O_2, and Ar balance in a flow rate of 50 mL/min (GHSV: 32 000 h^{-1}).

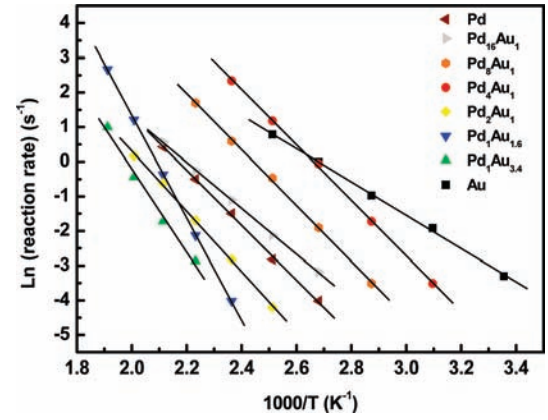

Figure 10. Arrhenius plots of the reaction rate (ln(*r*)) vs 1/*T* for CO oxidation over the SiO_2 supported Pd−Au alloy catalysts with a feed gas of 5.0 kPa CO, 5.0 kPa O_2, and Ar balance; about 5% CO conversion was obtained by diluting the catalysts with α-Al_2O_3 in a ratio range 1−20.

that unusually high activity of a Pd monomer for the catalytic reactions, such as VA synthesis by Pd−Au alloy catalysts, was derived from an ensemble effect, in which Au plays a role of isolating surface Pd atoms. We argue that those conclusions from the model catalysts are partly evidenced by the direct observation of metal vacancies in the real Pd−Au catalysts through HRTEM. As shown by Figures 3−6, a great number of Pd vacancies can be clearly seen in the Pd−Au alloys, indicating a decrease in Pd domains in the surface that may lead to the production of isolated Pd sites. An earlier study on Pd−Au alloy wires[51] revealed that the surface CO coverage decreased drastically from 0.5 over a pure Pd to 0.04 over a Pd (83 wt %)−Au (17 wt %) wire. Similar results have been obtained from Pd and Pd−Au films[2] and are believed due to the creation of isolated surface Pd atoms suggested by the X-ray

(51) Han, Y.-F.; Kumar, D.; Goodman, D. W. *J. Catal.* **2005**, *230*, 362.

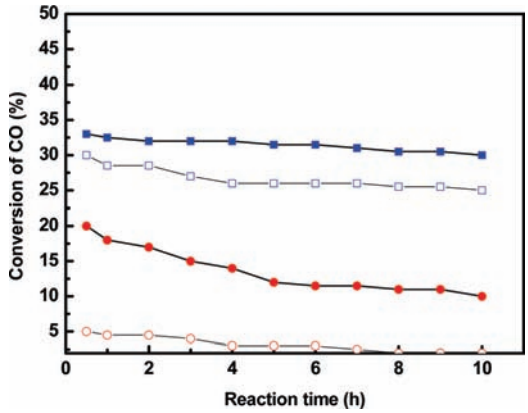

Figure 11. Time-dependent CO oxidation over the Pd_4Au_1/SiO_2 (■ and □) and Au/SiO_2 (● and ○; diluting 1:4 with α-Al_2O_3) catalysts in an ideal exhaust gas (filled symbols) of 5.0 kPa CO, 5.0 kPa O_2, and Ar balance and in an simulated exhaust gas (hollow symbols) of 5.0 kPa CO, 5.0 kPa O_2, 10.0 kPa H_2O, 20.0 kPa CO_2, and Ar balance, respectively, at a flow rate of 50 mL/min at 353 K.

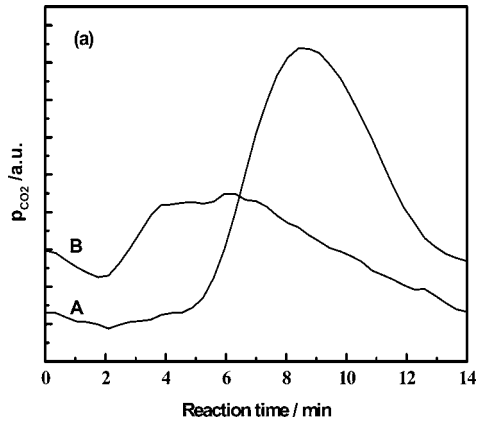

Figure 12. (a) CO_2 evolution profile for CO oxidation on the reduced Pd_4Au_1/SiO_2 catalyst at 300 K: on an O-precovered surface in flow of CO (5.0 kPa) + Ar (curve A), and on a CO-precovered surface in feed of O_2 (5.0 kPa) + Ar (curve B).

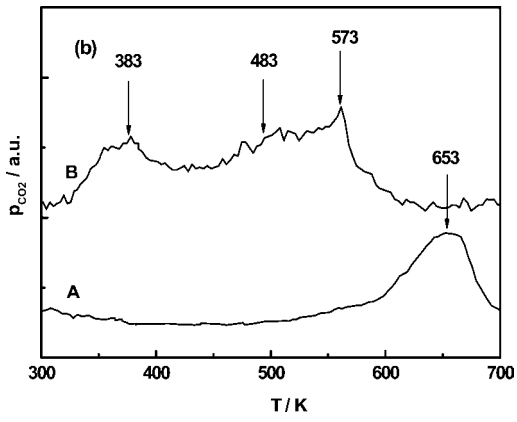

Figure 13. CO_2 evolution in the CO-TPD experiment on the reduced Pd/SiO_2 catalyst (curve A), and on the reduced Pd_4Au_1/SiO_2 catalyst (curve B).

absorption spectroscopy (XAS)[52] and infrared reflection absorption spectroscopy (IRAS)[18] that significantly decreases the number of active sites. In this study, DRIFTS diminution of the band at 2114 cm^{-1} (linear CO−Au or CO−Au/Pd bond) and the shift of the band from 2090 to 2080 cm^{-1} (linear CO−Pd bond) with increasing Au content from pure Pd to $Pd_1Au_{3.4}$ indicate the surface Pd atoms are gradually isolated by Au.

However, other studies on model catalysts including the TRSR results from single crystal Pd (100) and Pd−Au alloy wires[52,53] and the TPSR experiments (Figures 12 and 13) suggest that only alloyed Pd, and not Au, has the ability to chemisorb molecular oxygen irreversibly at/above 300 K. Therefore, a bifunctional mechanism is assumed to be responsible for CO oxidation, in which O_{ads} (and/or CO_{ads}) migrates from Pd to neighboring atoms or Au clusters through "spillover", as represented by eqs 3−6, in a mechanism similar to an electro-oxidation of CO.[54] This could be termed the "mixed metal" case, with the key factor being exchange of surface oxygen between Pd and Au as expressed by eq 5:

$$Pd + CO \rightarrow Pd{-}CO \quad (3)$$

$$Pd + O \rightarrow Pd{-}O \quad (4)$$

$$Pd{-}O + Au \rightarrow Pd + Au{-}O \quad (5)$$

$$Au{-}O + Pd{-}CO \rightarrow Au{-}Pd + CO_2 \quad (6)$$

(ii) The addition of Au alters the electronic (adsorptive) property of Pd surfaces due to crystallographic alloying and phase separation (Figure 1) that changes the Pd 3d and Au 4f core levels (Figure 7) and vibrational frequencies of CO−Pd bonds (Figure 8). CO is supposed to be preferentially adsorbed on Pd surrounded by Au atomic ensembles, as indicated by the band at 2114 cm^{-1} that appeared for $Pd_1Au_{1.6}$ and $Pd_1Au_{3.4}$,[15,19−21] and changes in CO−Pd and O−Pd bond strengths may kinetically favor CO oxidation. The hollow-core nanospherical structure and separated 3-atomic-line superlattice observed for nanoalloys (Figures 4 and 6) indicate the surface Pd atoms should be highly dispersed as compared to pure Pd. As a result, a large number of Pd active sites with low coordination number may be created in alloy surfaces, especially by the interaction with Au atoms. In particular, based on the activity comparison, the Pd ensemble in Pd_4Au_1 (the CO−Pd bond of 2090 cm^{-1}) is an optimal structure that may be suitable for CO adsorption and activation, because more defects were probably produced as compared to other samples. This may account for the greater CO oxidation at elevated temperatures (>373 K) over Pd−Au alloys, as compared to monometallic Pd catalysts, when supported on TiO_2 and SiO_2.[2−8] Alternatively, Au atoms surrounding surface Pd atoms may prevent Pd aggregation and lead to higher stability of Pd_4Au_1 over Au-only (Figure 11).

However, overloading Au in Pd−Au alloys increases the energy barrier (from 66.5 to 100 kJ/mol) toward CO oxidation (Figures 9 and 10), because more surface Pd atoms are obscured by Au. This interpretation is consistent with the increase of band intensity at 2114 cm^{-1} (linear CO−Au/Au−Pd bond) in passing from Pd_2Au_1 to $Pd_1Au_{3.4}$ due to blocking of the adsorption/migration of CO_{ad}/O_{ad} during reaction.

Further exploration of Pd−Au alloys toward low-temperature reactions and the role of Au-mediated chemical and structural modifications is in progress, as these materials may prove highly efficient for the partial oxidation of hydrocarbons and the

(52) Gorodetskii, V. V.; Matveev, A. V.; Podgornov, E. A.; Zaera, F. *Top. Catal.* **2005**, *32*, 17.
(53) Eley, D. D.; Moore, P. B. *Surf. Sci.* **1981**, *111*, 325.
(54) Davis, R. J.; Boudart, M. *J. Phys. Chem.* **1994**, *98*, 5471.
(55) Canning, N. D. S.; Outka, D.; Madix, R. J. *Surf. Sci.* **1984**, *141*, 240.
(56) Gossner, K.; Mizera, E. *J. Electroanal. Chem.* **1979**, *98*, 37.

combustion of organic compounds. Such functionality is urgently needed for environmental protection.

4. Conclusions

Pd−Au nanoalloy particles deposited on silica supports separate into biphasic assemblages of Pd-rich and Au-rich alloys over the entire compositional range between the pure metals. The solubility limit of Au in Pd was 12 at. %, while 31 at. % of Pd substitutionally replaced Au. The alloy pairs appeared in proportions consistent with the bulk composition of the catalyst. At Pd-rich compositions, hollow spheres or annular morphologies form, while Au-rich crystals were often twinned. Surface defects, ascribed as metal vacancies, were directly observed and contribute to enhanced low-temperature CO oxidation. The abundance and possible role of alloy superstructures arising from Pd/Au ordering are yet to be assessed. Alloying electronically modifies Pd and Au elements, shifting the Pd_{3d} and Au_{4f} core-levels and promoting charge transfer between Pd and Au, in a manner that favors CO absorption. Furthermore, the growth of the band at 2114 cm^{-1} with rise in Au content in Pd−Au alloys, which is attributed to the linear CO−Au or CO−Au/Pd, suggested that Pd atoms in the surface might be surrounded or separated by Au. Pd−Au alloy catalysts showed significant activity and stability toward low-temperature CO oxidation even at 300 K for bulk compositions from Pd to Pd_4Au_1, but showed degraded performance at higher Au contents due to higher activation that is accompanied by greater surface coverage by coverage of Au.

On the basis of those results, Au effects on Pd electronic properties are assumed to pertain to the origin of novel catalyst activity of Pd−Au alloys. As a consecutive effort on the research and development of the next generation of catalysts, we expect that the insights obtained in this study can inspire people to prepare or design novel nanoalloy catalysts suitable for low-temperature catalytic combustion and selective oxidation. Also, this work is very meaningful for sustainable economic development, especially currently as we are facing the hiking of the globe oil price.

Acknowledgment. The authors are grateful for the support from the Chinese Education Ministry 111 Project (B08021), the Non-Government International Cooperation Project of Shanghai Ministry of Science and Technology (2010/10230705900), Shanghai PuJiang Talent Program (2010/10PJ1402500) and Fundamental Research Funds for the Centred Universities.

JA102617R